Magnetization Reversal in a Novel Gradient Nanomaterial

T. C. Ulbrich,[1,*] D. Makarov,[1] G. Hu,[2] I. L. Guhr,[1] D. Suess,[3] T. Schrefl,[4] and M. Albrecht[1]

[1]*University of Konstanz, Department of Physics, D-78457 Konstanz, Germany*
[2]*Hitachi San Jose Research Center, San Jose, California 95120, USA*
[3]*Institute for Solid State Physics, Vienna University of Technology, 1040 Vienna, Austria*
[4]*Department of Engineering Materials, University of Sheffield, S1 3JD, United Kingdom*

(Received 2 September 2005; published 21 February 2006)

The deposition of Co/Pd multilayer films onto self-assembled particle arrays with particle sizes down to 50 nm leads to pronounced curvature-induced physical properties. Unlike in classical nanosystems, the so-formed single caps on top of the spherical particles exhibit a radial symmetric anisotropy orientation across their surface. Its impact on the magnetization reversal process was analyzed experimentally for different particle sizes and compared to micromagnetic simulations, offering new opportunities in the functionalization of magnetic nanostructures.

DOI: 10.1103/PhysRevLett.96.077202 PACS numbers: 75.75.+a, 75.60.Jk

The rapid advance in fabricating nanostructures with controlled size and shape offered by modern lithography techniques has triggered increased research in magnetic nanostructures. In this regard, the magnetization reversal mechanism is of particular interest. Apart from its crucial technological importance, its control is interesting from a fundamental point of view since the specific magnetic and geometrical properties of a nanostructure are likely to cause significant alterations. Numerous investigations, employing different shapes of structures such as squares, ellipses, and disks [1–8] have been reported. In contrast to these nanostructures, a novel nanomaterial, which consists of a multilayer film on top of a spherical particle, was introduced recently in Ref. [9]. This system is distinct from the classical geometries typically investigated: Neither extrinsic nor intrinsic properties are uniform in space. The film is extended over a wide region of the sphere and thus shows substantial curvature. The film thickness varies and so do the intrinsic magnetic properties, most notably the magnetic anisotropy, which is a key factor affecting the fundamental nature of the reversal process. The realization of such a system is possible because Co/Pd multilayered films show a strong perpendicular magnetic anisotropy that originates primarily from interface contributions due to the asymmetry of Co and Pd layers perpendicular to the interface [10–12]. Thus, the anisotropy axis will always point perpendicular to the particle surface. Assuming an evaporation direction perpendicular to the substrate surface, the thickness d of the Co and Pd layers is highest at the top of the particle and reduces towards the sides with $d \sim \cos\varphi$, where the angle φ designates the position on the particle surface with respect to the deposition direction. Since a typical Co layer thickness of 0.3 nm corresponds to only about 1.5 monolayers, we expect the ferromagnetic properties of the multilayer stack to be suppressed for an angle φ higher than about 50°, where the Co layer thickness drops below one monolayer, starting to form a dilute Co-Pd alloy without significant anisotropy and moment. As a consequence, this effect leads to exchange isolation of the magnetic caps.

In this Letter, we report the specific magnetic characteristics of such a gradient nanomaterial, in particular, its impact on the reversal mechanism. Angle-dependent reversal studies were performed for different particle sizes and the experimental results are interpreted using micromagnetic simulations.

The nanostructure samples were prepared using a topographic pattern formed of self-assembled densely packed polystyrene particles with diameters of 50, 110, and 310 nm. Onto these particle monolayers Co/Pd multilayer films were deposited at room temperature as reported in Ref. [9]. The multilayer film consisted of a $[\mathrm{Co}(0.3\ \mathrm{nm})/\mathrm{Pd}(0.8\ \mathrm{nm})]_8$ stack grown on a 3 nm-thick Pd seed layer and was covered with an additional 0.8 nm-thick Pd capping layer to prevent oxidation.

The topographic assembly as well as the specific morphology of the deposited films were investigated by atomic force (AFM) and scanning tunneling microscopy (STM). While the AFM image shown in Fig. 1(a) confirms a densely packed particle assembly for the 50 nm particles, the STM image in Fig. 1(c) reveals a grainy structure of the deposited film stack with grain diameters of about 6 nm. A root-mean-square roughness of about 0.8 nm was obtained by height profile measurements along the surface [Fig. 1(d)]. Similar studies on assemblies with larger particle sizes show basically the same film morphology, indicating that the underlying microstructure of the individual grains is also similar. This suggests that similar magnetic properties such as the magnetic anisotropy that are connected to the microstructure of the grains are present. Note that as long as the grain size is much smaller than the particle diameter, the grains can be assumed as locally planar entities distributed on a curved surface. However, due to the difference in curvature for different particle sizes the spatial variation in material properties along the spherical surface such as layer thickness and

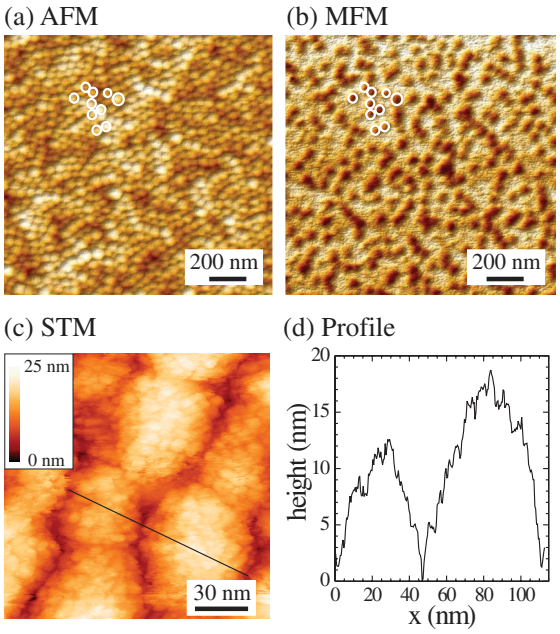

FIG. 1 (color). (a) AFM and (b) corresponding MFM image of an array with magnetic caps on 50 nm particles after applying a perpendicular reverse field to the initially saturated sample. Several individually reversed particles are highlighted. (c) STM image of caps formed on 50 nm particles, revealing the deposited film morphology. A height profile along the marked path is shown in (d).

anisotropy orientation changes drastically. In contrast, STM images on a reference sample, where the multilayer stack was evaporated on a plain sapphire substrate, revealed grain sizes in the order of 20 nm, indicating improved growth conditions with presumably sharper interfaces and thus higher anisotropy values as compared to the grains on the caps.

Local magnetic properties were investigated by magnetic force microscopy (MFM). Figure 1(b) shows a MFM image after applying a perpendicular reverse field of about 0.25 T (close to the coercivity field) to the initially saturated sample. Individually reversed caps (dark contrast) are observable, revealing a quasi–single-domain remanent state with an average magnetization orientation pointing perpendicular to the substrate. In this case, each cap is switched independently during the reversal process, indicating that the caps are strongly exchange decoupled.

To obtain more information on the magnetic properties, measuring the angular dependence of the nucleation field has been widely used to characterize the magnetization reversal mechanism. The magnitude of the switching field is either Stoner-Wohlfarth–like (S-W) with a minimum at around 45° for nucleation dominated magnets or increases as $1/\cos\theta$ in pinning type magnets [13], where θ refers to the angle of the external field with respect to the substrate normal. For both coherent rotation and nucleation, the angle dependence of the switching field follows S-W behavior, showing a minimum of the magnitude of the switching field at a field angle of 45°, unless domain wall pinning occurs. Here on the nanocap arrays, polar magneto-optical Kerr effect measurements were carried out using a focused laser beam with a spot size of 40 μm. All loops used in this work are remanent loops, which means that the polar Kerr rotation indicating the perpendicular component of the magnetization is detected in remanence after removing the applied reverse field. Note that before applying a reverse field, the sample is always saturated. The switching field H_s is defined as the field required to reverse the magnetization of half the caps in the probed ensemble. To obtain information on the reversal mechanism, H_s was measured as a function of applied field angle θ. The normalized switching field is plotted in Fig. 2(a) versus the angle θ. After a rapid decrease for small angles θ, the magnitude of the switching field for the caps on the 50 nm particles has a broad minimum from $\theta =$ 45° to 80° [9]. Reversal studies on larger particles reveal a different behavior, showing a little drop in H_s for the 110 nm particles or a small increase for the 310 nm particles towards higher angles, indicating a domain-wall-motion-controlled reversal mechanism. This behavior differs substantially from the S-W model, plotted as a solid line in Fig. 2(b), which is applicable to single-domain particles with uniaxial anisotropy reversing via coherent rotation [14].

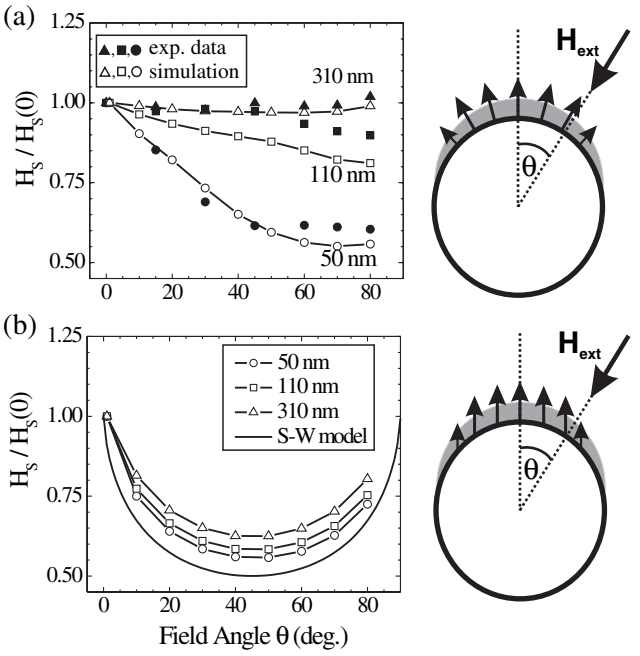

FIG. 2. Normalized switching field as a function of applied external field angle θ (a) from experimental data and simulations with spatial anisotropy distribution for all particle sizes and (b) from simulations for caps assuming uniaxial anisotropy, including a representation of the Stoner-Wohlfarth model. The solid lines serve as a guide to the eye for the simulated data points. Included are schematics of the magnetic caps showing the local anisotropy distribution and the external field direction.

To investigate the physical origin of this remarkable behavior in detail, micromagnetic simulations were performed, enabling us to distinguish the influence of the anisotropy distribution, the change in magnitude of anisotropy, and the dependence on size (curvature). The theoretical treatment of magnetization dynamics at zero temperature starts from the Gilbert equation [15]

$$\frac{\delta \mathbf{M}}{\delta t} = -|\gamma|\mathbf{M} \times \mathbf{H}_{\text{eff}} + \frac{\alpha}{M_s}\mathbf{M} \times \frac{\partial \mathbf{M}}{\partial t},$$

which describes the physical path of the magnetic polarization $\mathbf{M}$ towards equilibrium. γ is the gyromagnetic ratio of the free electron spin. The damping constant α considers the relaxation towards equilibrium phenomenologically. The effective field $\mathbf{H}_{\text{eff}}$ is the negative functional derivative of the total magnetic Gibbs free energy,

$$E = \int \left(\frac{A}{M_s^2}(\nabla \mathbf{M})^2 - \frac{K_u}{M_s^2}(\mathbf{M} \cdot \mathbf{u})^2 - \frac{\mu_0}{2}\mathbf{H}_d \cdot \mathbf{M} - f_{\text{zee}} \right) dV,$$

which is the sum of the exchange energy, the magnetic anisotropy energy, the magnetostatic energy, and the Zeeman energy. Here A is the exchange constant, K_u the magnetic anistropy constant, $\mathbf{u}$ the direction of the easy axis, H_d the self-demagnetizing field, and f_{zee} the Zeeman energy density. For complex particle shapes and space varying material parameters, such as the anisotropy constant K_u and the spontaneous polarization M_s, numerical schemes are required. The finite element method is suitable for spatial discretization of the micromagnetic equations [16], where the demagnetizing field is derived from a scalar potential. To transform the boundary condition of zero potential at infinity to the boundary of the magnetic region, the hybrid finite element or boundary element method was applied [17]. In order to implement the properties of the magnetic caps, the volume was divided into a mesh of finite elements with a maximum side length of 5 nm. The magnetic anisotropy vector of each finite element points in radial direction. For $0° < \varphi < 50°$ the magnitude of magnetic anisotropy, saturation magnetization and exchange constant of the individual elements is set to constant values, K_u^0, M_s^0, and A^0, respectively, since the thickness of the single Co layers changes from about 1.5 to 1 monolayer. To account for the change of the anisotropy with Co thickness, K_u^0 has to be considered as an effective value, which will be reduced compared to the value measured on a plane reference film sample. For higher angles both anisotropy and saturation magnetization are approximated by a Gaussian function [$f(\varphi) = \exp(-(\frac{\varphi-\varphi_0}{\sigma})^2)$ with $\varphi_0 = 50°$ and $\sigma = 0.1$], leading to a steep drop in $K_u(\varphi)$ and $M_s(\varphi)$ to zero. Note that the anisotropy distribution is pointing perpendicular to the particle surface and its absolute value is assumed to be independent of particle size as long as the particle diameter is larger than the grain size of the deposited film. A schematic cross section of the model is depicted in Fig. 2(a) sketching the distribution of the anisotropy orientation and also its local magnitude variation. The switching field H_s was extracted from the sign change of the magnetization component perpendicular to the substrate surface. Since only equilibrium conditions were investigated, the damping constant was set to 1.

Single particle hysteresis loops were simulated for different particle sizes and various directions of the external field with $A^0 = 1 \times 10^{-11}$ J m^{-1} and $M_s^0 = 0.5$ MA m^{-1}. K_u^0 is the fitting parameter for the simulations. The normalized best fit results using one single K_u^0 value are compared to the experimental data and presented together in Fig. 2(a). Best fits were obtained with $K_u^0 = 0.3$ MJ m^{-3}, which is 75% of the measured film value. The latter is consistent with the improved film quality expected for the used reference sample, which is known to increase the magnetic anisotropy in Co/Pd multilayer films [18]. For all particle sizes there is good agreement between simulations and experiment, clearly verifying the assumptions.

The equilibrium spin configuration at various external fields for different field directions can be extracted from the simulations as shown in Fig. 3(a) for the magnetic caps on 310 nm particles, providing a detailed picture of how the local magnetization evolves during reversal. We observe a domain wall dominated switching process, in which an initial ring domain nucleates at an angle of about 45° relative to the external field. At this angle a minimal nucleation field is required, as suggested by the S-W model. The z component of the magnetization in Fig. 3(a) shows that the nucleation of a reversed domain (blue) is preceded by the formation of a domain with the magnetization at 90° to the remanent magnetization direction (green). The x and y components are then maximal, revealing radial symmetry. The nucleus (blue) is not local-

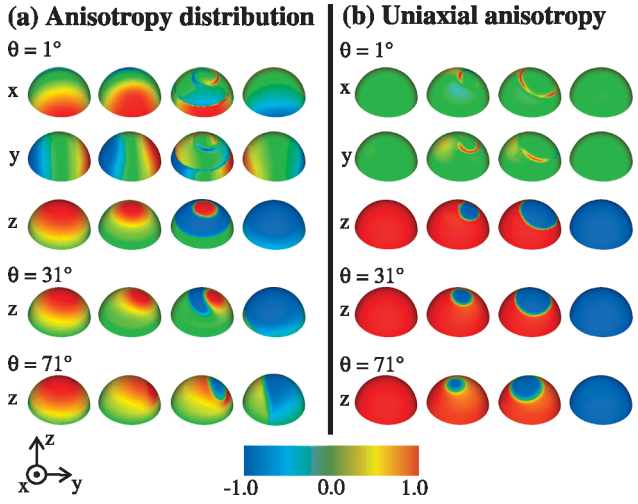

FIG. 3 (color). Normalized magnetization of the z component of the caps shown in color code for the case of (a) spatial distribution in the anisotropy and (b) uniaxial anisotropy for caps on 310 nm spheres and various directions of the applied field. Within a sequence the external field is increased from left (zero field state) to right, and representative states are chosen. Additionally, the x and y components are given for $\theta = 1°$.

ized but spread over the entire structure, leading to a three-domain configuration during magnetization reversal of the 310 nm cap. It can be concluded that exchange coupling between the initial formed domain with zero z magnetization and the remainder of the particle will lower the nucleation field for building a reversed nucleus and lead to the immediate growth of the reversed domain. The position of the initially nucleated domain follows the direction of the external field. Since various anisotropy directions are available in the cap for the nucleation process, only a weak angle dependence is expected. While the caps on the 110 nm particles show a similar behavior, the reversal mechanism of the smallest caps depends strongly on the applied field direction. For small angles the process resembles that described above. However, at higher angles reversal occurs neither via an obvious domain wall motion nor by coherent rotation. It might be more suitable to describe the reversal process as domain smearing. Moreover, the magnetization within the cap is strongly exchange coupled. Thus, the application of an external field at around zero degree will lead to locking of the remanent state. In addition to the anisotropy field the magnetic moments at the top of the sphere see an exchange field provided by the already tilted magnetic moments of the surrounding ring of the domain with 90° magnetization. Increasing the angle of the external field breaks the symmetry and thus weakens the locking mechanism. As a consequence the switching field decreases.

To prove the importance of the anisotropy distribution, additional simulations were performed by applying a uniaxial anisotropy perpendicular to the substrate surface for all finite elements. All other parameters were unaltered. This model and the results of the simulations are given in Fig. 2(b). The data compare rather well with S-W behavior and suggest a more coherent reversal process for all sizes. However, as can be seen in Fig. 3(b) for the 310 nm particles the initial domain nucleation is localized roughly in the center of the cap for all angles, where the highest demagnetization field is present, followed by domain wall propagation. This reversal process is clearly not via coherent rotation, thus proving that a S-W–like angle dependence does not, in general, imply a coherent rotation reversal mechanism. In our case, the reversal is governed by a nucleation event which has S-W characteristics, followed by domain wall motion which causes the entire structure to reverse. Experimental evidence for this behavior was recently reported on planar magnetic micrometer-size structures with uniaxial anisotropy [19].

In conclusion, while most thin film systems are globally planar with uniform properties, film deposition on a curved surface, where the topological change can alter the film properties locally, could have far reaching implications in the physics of nanoscale magnetism. In contrast to classical magnetic nanostructures with uniaxial anisotropy, the angular dependence of the switching field of the nanocaps follows neither the Stoner-Wohlfarth behavior nor the $1/\cos$ law. Here, the magnetization reversal is driven by collective processes induced by the radial symmetric spatial variation of anisotropy orientations, which significantly alter the reversal process. This process depends strongly on the curvature of the particles which determines the spatial gradient in the material properties, which can be further tailored, providing novel functionality of the nanostructures.

The authors like to thank W. Evenson, O. Hellwig, G. Schatz, P. Leiderer, and J. Boneberg for fruitful discussions. Financial support was provided by the Deutsche Forschungsgemeinschaft through the Emmy-Noether program and the SFB 513, and the Austrian Science Fund (Y132-N02).

*Electronic address: till.ulbrich@uni-konstanz.de

[1] R. P. Cowburn, A. O. Adeyeye, and M. E. Welland, Phys. Rev. Lett. **81**, 5414 (1998).
[2] X. Zhu, P. Grütter, V. Metlushko, and B. Ilic, Phys. Rev. B **66**, 024423 (2002).
[3] M. Hehn, K. Ounadjela, J.-P. Bucher, F. Rousseaux, D. Decanini, B. Bartenlian, and C. Chappert, Science **272**, 1782 (1996).
[4] R. P. Cowburn, D. K. Koltsov, A. O. Adeyeye, M. E. Welland, and D. M. Tricker, Phys. Rev. Lett. **83**, 1042 (1999).
[5] J. Sort, A. Hoffmann, S.-H. Chung, K. S. Buchanan, M. Grimsditch, M. D. Baro, B. Dieny, and J. Nogues, Phys. Rev. Lett. **95**, 067201 (2005).
[6] S. P. Li, D. Peyrade, M. Natali, A. Lebib, Y. Chen, U. Ebels, L. D. Buda, and K. Ounadjela, Phys. Rev. Lett. **86**, 1102 (2001).
[7] T. Shinjo, T. Okuno, R. Hassdorf, K. Shigeto, and T. Ono, Science **289**, 930 (2000).
[8] C. A. F. Vaz, L. Lopez-Diaz, M. Kläui, J. A. C. Bland, T. L. Monchesky, J. Unguris, and Z. Cui, Phys. Rev. B **67**, 140405(R) (2003).
[9] M. Albrecht, G. Hu, I. L. Guhr, T. C. Ulbrich, J. Boneberg, P. Leiderer, and G. Schatz, Nat. Mater. **4**, 203 (2005).
[10] D. G. Stinson and S.-C. Shin, J. Appl. Phys. **67**, 4459 (1990).
[11] J. I. Hong, S. Sankar, A. E. Berkowitz, and W. F. Egelhoff, Jr., J. Magn. Magn. Mater. **285**, 359 (2005).
[12] P. F. Carcia, A. D. Meinhaldt, and A. Suna, Appl. Phys. Lett. **47**, 178 (1985).
[13] K. R. Coffey, T. Thomson, and J.-U. Thiele, J. Appl. Phys. **93**, 8471 (2003).
[14] E. C. Stoner and E. P. Wohlfarth, Philos. Trans. R. Soc. London **240**, 599 (1948).
[15] T. L. Gilbert, Phys. Rev. **100**, 1243 (1955).
[16] J. Fidler and T. Schrefl, J. Phys. D **33**, R135 (2000).
[17] D. R. Fredkin and T. R. Koehler, IEEE Trans. Magn. **26**, 415 (1990).
[18] Y. P. Lee, S. K. Kim, J. S. Kang, Y. M. Koo, J. I. Jeong, J. H. Hong, and H. J. Shin, J. Magn. Magn. Mater. **126**, 316 (1993).
[19] B. D. Terris, M. Albrecht, G. Hu, T. Thomson, and C. T. Rettner, IEEE Trans. Magn. **41**, 2822 (2005).